Large eddy simulations of energy dissipation due to backwash flows in wave overtopping

C. Sandoval and T. Stoesser

Abstract—**Wave energy is a source of renewable energy offering large power in the oceans to be harvested. Overtopping wave energy converters (OWEC) operate on the shore, facilitating relatively easy construction and maintenance. They can be integrated into coastal defence schemes, sharing the cost of construction and their environmental impact. The effectiveness of OWECs relies on their ability to capture large wave-overtopping volumes. The geometry of the run-up ramp plays an essential role in the efficiency of an OWEC. When an incoming wave approaches the run-up ramp, it crashes against the backwash, an interaction that affects the energy loss during the breaking of the wave. This study analyses the hydrodynamics during the backwash and its interaction with the next incoming wave on a sloped structure. A numerical code Hydro3D, based on Large Eddy Simulations, is used to carry out simulations. Two conditions are compared, one where no overtopping is allowed; the backwash is composed of the volume of water that run-up the structure and the second is a structure with a lower freeboard, allowing overtopping to occur which reduces the waves' backwash. The energy losses of these conditions are then evaluated. The findings of this study allows to verify if a reduction in the backwash can improve the efficiency of OWECs.**

Index Terms—**overtopping, wave, OWEC, LES**

I. Introduction

WAVE energy has great potential to be used as a sustainable source of green energy. Several projects have proven that harvesting energy from the wave action is possible [1], [2]. The locations with substantial wave energy resources are located in deep water and exposed to extreme conditions, [3], a fact that have made the development of this technology expensive and highly risky. Onshore wave energy converters like overtopping wave energy converters (OWEC) and oscillating water columns (OWC) offer a cheaper alternative to harvest wave energy. Because these devices operate on land, their costs of construction, maintenance, and operation are significantly lower than for deep and intermediate water depth energy converters. Another significant positive characteristic of on-shore devices is that they can be integrated into existing or new coastal defence schemes, sharing the cost of construction and their environmental impact and creating new benefits from the coastal defence. However, the efficiency of these devices needs to be improved to become an attractive and feasible solution for energy generation [2]. The present study is focused on OWEC and energy losses during wave breaking and run-up.

An OWEC is composed of three main parts: (i) the run-up ramp, where the water is captured and the transformation from kinetic energy to potential energy occurs; (ii) a reservoir, or more than one in the case of a multilevel OWEC, where the water is kept at a higher elevation compared to the mean water level; and (iii) the turbine which transforms the flow of energy into electricity. The design of each one of these pats affect the efficiency of the wave energy converter.

The efficiency of an OWEC relies strongly on its ability to capture large wave-overtopping volumes; that's why the overtopping discharge is commonly used as an indicator of the performance of an OWEC, [4], [5].

Large energy losses occur on the run-up ramp due to three main processes: (i) the collapse of the wave, (ii) the run-up and (iii) the backwash (run-down) which interferes with and decelerates the run-up. The energy dissipation in the first two processes directly affects the total volume of water that will overtop the structure. Several studies have analysed the importance of the ramp's geometry in the efficiency of an OWEC, [4]–[7], verifying that the performance of an OWEC can be affected by changing its geometry, for instance curved slopes or adding converging walls.

In a typical operation of an OWEC, the backwash flow is composed of the water that didn't overtop and then runs down the slope due to gravity back into the sea. This flow interacts with and impedes the incoming wave, affecting the energy dissipation during the collapse of the wave. Studies have mentioned the impact of the backwash flows on the overtopping discharge [8]. However, no detailed analysis of the wave-backwash interaction has been reported in the literature.

The study will be conducted with the numerical code Hydro3D-NWT, [9]. This tool is based on a Large Eddy Simulation (LES) methodology that allows obtaining instantaneous flow parameters. This type of numerical code is capable of simulating directly the large turbulent structures that account for most of the energy dissipation in the flow. Hydro3D-NWT have proven to be able to predict complex wave-structure interactions reproducing with accuracy the water surface, particle

The first author is funded by National Agency of Research and Development (ANID), Chilean Government.

Simulations were carried out on UCL's supercomputer Kathleen, support and computing time are gratefully acknowledged.

C. S. is with Department of Civil, Environmental and Geomatic Engineering, University College London, Gower Street, WC1E 6BT, London, UK (e-mail: claudio.sandoval.19@ucl.ac.uk).

T. S. is with Department of Civil, Environmental and Geomatic Engineering, University College London, Gower Street, WC1E 6BT, London, UK (e-mail: t.stoesser@ucl.ac.uk).

Digital Object Identifier: https://doi.org/10.36688/ewtec-2023-626

velocities, and pressures [9], [10].

In the present study, an evaluation of the impact of the backwash flow on energy dissipation is conducted by comparing a scenario with no overtopping with one where the structure's freeboard is such that wave overtopping occurs. These two cases allow creating different levels of backwash flows, permitting to assess the impact of this flow on the efficiency of a OWEC.

II. Numerical framework

Hydro3D-NWT is an open-source code based on the large eddy simulation (LES) methodology. Here the main elements of the code are presented. More details of Hydro3d-NWT can be found in [9].

Hydro3D-NWT solves the unsteady, incompressible, viscous, spatially-filtered Navier-Stokes equations:

$$\frac{\partial \bar{u_i}}{\partial x_i} = 0 \tag{1}$$

$$\frac{\partial \bar{u_i}}{\partial t} + \frac{\partial \bar{u_i}\bar{u_j}}{\partial x_j} = -\frac{1}{\rho}\frac{\partial \bar{p}}{\partial x_i} + \frac{\partial}{\partial x_j}(\nu \frac{\partial \bar{u_i}}{\partial x_j}) - \frac{\partial \tau_{ij}^{SGS}}{\partial x_j} + f_i + F_i^{sf} + g_i \tag{2}$$

where: $\bar{u_i}$ is the instantaneous filtered velocity in the x_i direction and $\bar{p}$ the pressure field. ρ and ν are the fluid density and kinematic viscosity, respectively and τ_{ij}^{SGS} the sub-grid scale (SGS) stress tensor. f_i is the forcing term of the immersed boundary method acting on the fluid, F_i^{sf} is the surface tension, and g_i the gravitational acceleration.

A staggered uniform Cartesian grid is used discretised (1) and (2). There the scalar quantities are calculated in the centre of the cell, and the velocities and derivatives are in the centre of each face. The convective term of (2) (left side) is calculated using a 5^{th} order weighted essentially non-oscillatory (WENO) scheme [11], whereas the diffusive terms are solved using a 2^{nd} order central differences (CDS).

The time advance is achieved by the fractional-step method, [12], with a 3^{rd} order Runge-Kutta (RK) scheme. The present study uses a variable time step with a Courant-Friedrichs-Lewy (CFL) criterion set to a maximum of 0.1.

LES requires a subgrid-scale model (SGS) to account for the small-scale eddies that are not solved in the grid. This model removes energy from the flow. In Hydro3D-NWT, the Wall-Adapting Local Eddy viscosity (WALE) is implemented [13]. This method uses the velocity tensor $\bar{g_{ij}} = \frac{\partial \bar{u_i}}{\partial x_j}$ to calculate ν_t as:

$$\nu_t = (C_w \Delta)^2 \frac{(S_{ij}^d S_{ij}^d)^{3/2}}{(\bar{S_{ij}}\bar{S_{ij}})^{5/2} + (S_{ij}^d S_{ij}^d)^{5/4}} \tag{3}$$

C_w is the WALE empirical constant set to $C_w = 0.46$, δ is the size of the filter width calculated as $(dx \cdot dy \cdot dz)^{1/3}$.

The water surface is captured using the Level Set Method (LSM), [14]. Here a function ϕ is defined equal to zero in the interface between air and water (Γ), positive in the volume occupied by water (Ω_{water}) and negative in the air (Ω_{air}). The magnitude of this function represents the distance of the location to the interface.

$$\phi(x,t) = \begin{cases} < 0, & \text{if } x \in \Omega_{air} \\ = 0, & \text{if } x \in \Gamma \\ > 0, & \text{if } x \in \Omega_{water} \end{cases} \tag{4}$$

A 5^{th} order weighted essentially non-oscillatory (WENO) scheme is used to discretise the spatial derivatives of ϕ.

A transition zone between air and water is used to avoid discontinuity in the fluid properties, density and dynamic viscosity near the interface. A Heaviside function $H(\phi)$ is used to smoothly transition between air and water. The function is applied in a layer of thickness 2ε, were $\varepsilon = 2max(dx, dy, dz)$

$$H(\phi) = \begin{cases} = 0, & \text{if } \phi < -\varepsilon \\ = \frac{1}{2}(1 + \frac{\phi}{\varepsilon} + \frac{1}{\pi} sin\frac{\pi\phi}{\varepsilon}), & \text{if } |\phi| \leq \varepsilon \\ = 1, & \text{if } \phi > \varepsilon \end{cases} \tag{5}$$

In Hydro3D-NWT structures are accounted for by the diffusive direct forcing IB method [15]. The solid geometry is defined by Lagrangian markers, where a force is introduced to enforce a non-slip condition at the solid-fluid interface. This force is interpolated to the fluid cells in the vicinity of the interface and included in (2) as f_i. The IB method follows the following general steps: First, the non-divergence velocity, u_i^*, calculated in the Eulerian fluid cell is interpolated to the nearest Lagrangian markers; Secondly, the force, f_{iL}, necessary to impose the non-slip condition in the market is evaluated; then f_{iL} is interpolated back to the fluid cell, f_i; and finally the velocity is update considering the new force introduced.

The surface tension is included in the fluid in the same transition layer defined in the LSM for the transition of the fluid properties. In that layer F_i^{sf} is calculated according to [16]:

$$F_i^{sf} = \sigma k \delta(\phi) n_i \tag{6}$$

Where σ is the surface tension coefficient, k is the curvature of the interface, and $\delta(\phi)$ is a function to smooth the surface force in a transition zone over the free surface. These parameters are defined according to the function ϕ used in the Level-Set Method (LSM) and according to the next formulation:

$$k = -\nabla n_i, \qquad n_i = \frac{\nabla \phi}{|\phi|} \tag{7}$$

and

$$\delta(\phi) \begin{cases} = \frac{1}{2}(1 + cos(\frac{\pi\phi}{\varepsilon}), & \text{if } \quad |\phi| < \varepsilon \\ = 0, & \text{if } \quad else. \end{cases} \tag{8}$$

Waves are generated at the west boundary of the domain, in a zone with a length equal to the wavelength, L_w. In this zone, the water surface elevation and the particle velocity of the fluid are computed according to the analytical solution of 2^{nd} order Stokes waves.

To reduce reflections from the west boundary, a relaxation zone is implemented with the same length as the wave generation part. The relaxation is achieved using the relaxation method (RM) described in [9]. A relaxation function $\Gamma(x_r)$ is defined to modify the water surface depth and velocities towards the analytical solution, Γ is a function of a secondary coordinate, x_r, which takes a value of zero at the end of the relaxation zone, $x = x_{er} = L_w$, and one at $x = 0m$.

$$\Gamma(x_r) = 1 - \frac{e^{x_r{}^R} - 1}{e - 1} \tag{9}$$

$$x_r = \frac{x_{er} - x_i}{x_{er}} \tag{10}$$

The coefficient R prescribe the rate of relaxation in the relaxation zone. A value of $R = 3.5$ is used in the present study. After Hydro3D-NWT computes the location of the free surface, this is updated by (11) inside the relaxation zone towards the analytical solution calculated with the corresponding wave theory. The same process is conducted for the velocities in every sub-step of the Range-Kutta scheme, (12).

$$\phi = \Gamma(x_r)\phi_{computed} + (1 - \Gamma(x_r))\phi_{analytical} \tag{11}$$

$$u_i = \Gamma(x_r)u_{icomputed} + (1 - \Gamma(x_r))u_{ianalytical} \tag{12}$$

III. Validation Wave Overtopping

The performance of an OWEC is related to the amount of water captured in each wave event. This is commonly measured with the wave overtopping mean discharge, q, defined as the water volume that overtops the structure over the total time.

In [5] the performance to capture wave overtopping in a two-level OWEC was studied with a scale physical model. The experiment was conducted in a wave flume at the Ocean University of China. Regular waves were used, with heights (H_w) of 0.05m, 0.075m and 0.1m, and wave period (T) of 0.8s, 1.0s, 1.2s and 1.4s. Three water depths (d) were used, 0.3m, 0.35m and 0.4m. The present study considers only the cases with the lower water level ($d = 0.3m$), which reported negligible water volumes in the upper reservoir. Therefore, only the lower section of the slope is simulated here. Three slope angles of the front ramp were explored $20°$, $30°$ and $40°$. The $30°$ structure is used in the present study because this slope is frequently used in coastal breakwaters. The crest of the reservoir was set to $0.35m$ with respect to the bottom of the flume.

Figure 1 shows the domain used in Hydro3D-NWT to reproduce the experiment. A $dx = 0.0035$, $dy = 0.005$ and $dz = 0.0025$ grid was found to accurately reproduce the water surface and avoid irregularity in the interface with the Lagrangian markets of the IB method.

Figure 2 shows one overtopping sequence for the wave condition $H_w = 0.05m$ and $T = 1.0s$ ($L_w = 1.37m$). Black lines present the water surface extracted from laboratory snapshots [17], and coloured areas

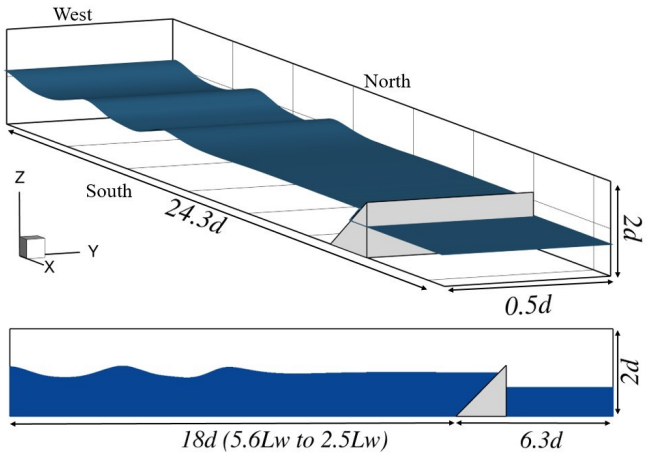

Fig. 1. Top: 3D view of domain and water surface, bottom: domain's longitudinal-section.

Hydro3D results. It can be seen that the numerical results match the time step of each stage. At T/4, the water surface adopts a convex shape due to the interaction with the slope, both in the laboratory and the simulation. The laboratory shows a near vertical end of the wavefront against the slope; in the simulation, that shape is not present, but a layer of water from the backwash is still on the slope. At T/2 the run-up reaches the crest of the structure; no overtopping has occurred yet. It is possible to observe that the run-up flow in the simulation is slower than in the laboratory. At 3T/4, the run-up spill into the rear side of the structure. In the simulations, the flow breaks down after the crest, a process that agrees with the laboratory description where the authors mention a separation in sub-fingers of the water flow. In the last snapshot, the backwash recedes faster in the laboratory; Hydro3D results still show a layer of water on the slope, which explains the difference in $T/4$.

A dimensionless overtopping discharge, Q, is used to evaluate the wave overtopping discharge in [5]. Q is a function of the mean discharge, q evaluated as the total volume captured in the first 15 waves over the total time, starting from the first overtopping event. The dimensionless discharge is calculated according to (13).

$$Q = \frac{q}{H_w\sqrt{gH_w}} \tag{13}$$

At the back of the structure, a lower water level is used to leave dry the area where the waves fluctuate. The overtopping flows are evaluated on the crest of the structure as the $f = \sum u_i A_{cell}$ where u is the horizontal velocity in the cell i and A_{cell} the cross-section of the fluid cell, x face.

Fig 3 shows the dimensionless overtopping, Q, calculated in [5], (green triangles) and results from Hydro3D (black squares), for the waves $H_w = 0.075m$, $T = 0.8s, 1.0s, 1.2s, 1.4s$ ($L_w = 0.96m, 1.37m, 1.77m, 2.15m$ respectively). Firstly, it can be seen that Hydro3D results capture the increasing trend of Q with L_w, however, overestimates the discharge for the longer waves, i.e. $L_w = 1.77m$ and $L_w = 2.15m$. Hydro3D is

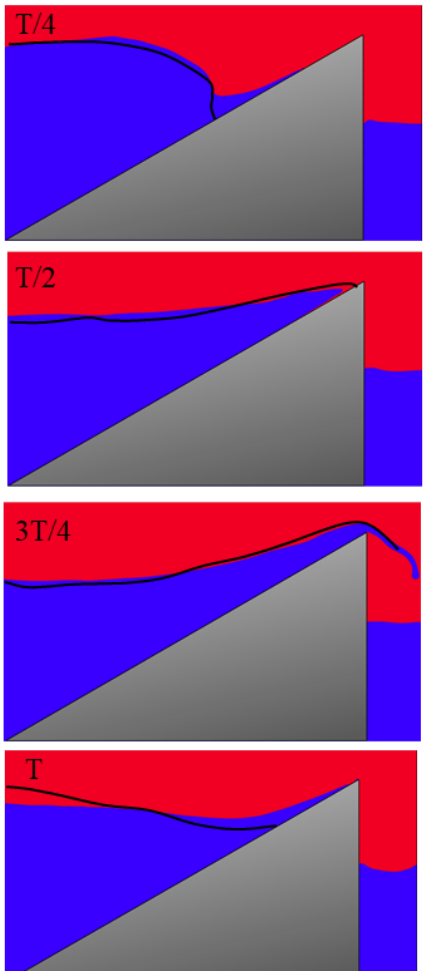

Fig. 2. Comparison wave evolution during one overtopping event, $H_w = 0.05m$ and $T = 1.0s$ ($L_w = 1.37m$). Slide Hydro3D-NWT and black line water surface from laboratory extracted from [17].

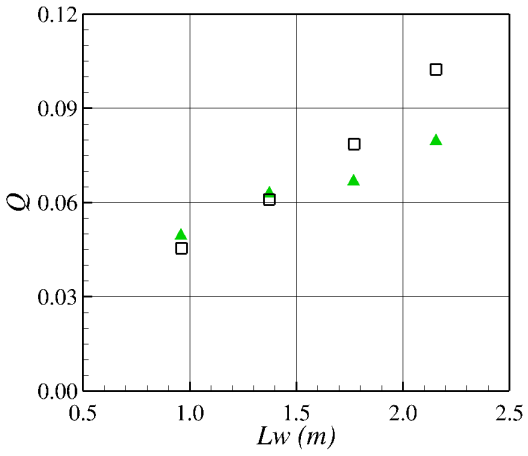

Fig. 3. Comparison dimensionless discharge for waves Hw=0.075m and 30° front slope. Green triangles laboratory data, [5], and black squares Hydro3D results.

able to estimate Q with good accuracy the discharge for the two shorter waves; a slight underestimation of 8.0% is calculated for the shorter wave and just 3.2% below the data for the $1.37m$ wave. For the wave, $L_w = 1.77$, Q is overestimated by $17,9\%$ approximately, which can be considered acceptable due to the high variability of the overtopping process. Hydro3D results

TABLE I
SIMULATION PARAMETERS, WAVE PERIOD T, WAVE LENGTH L_w, WATER DEPTH d, DIMENSIONLESS FREE BOARD R_c/H_w AND STRUCTURE SLOPE

Case	T (s)	L_w (m)	d (m)	R_c/H_w	Slope (°)
$case1_{08}$	0.8	0.96	0.3	2.6	30
$case2_{08}$	0.8	0.96	0.3	1/1.5	30
$case1_{10}$	1.0	1.37	0.3	2.6	30
$case2_{10}$	1.0	1.37	0.3	1/1.5	30

for the longer wave condition, $L_w = 2.15m$ exceed the laboratory results by 29%.

In the following section, the two shorter waves, for which the best match is achieved, are used to study the influence of the backwash on energy dissipation.

IV. BACKWASH AND ENERGY DISSIPATION

To evaluate the effect of the backwash flow on energy dissipation during the collapsing of the approaching wave, two addiotional simulations are carried out with Hydro3D, see Table I for details. Case 1 includes a structure high enough that no overtopping occurrs; therefore, the run-down volume of water is equal to the run-up volume of water. Case 2 is a structure with the same freeboard as used in the validation case, $R_c = H_w/1.5$, which allows the occurrence of overtopping. In this case, the run-down volume of water is less than the run-up volume. These two scenarios with different backwash volumes but the same incoming waves allows for analysing how the backwash affects the energy dissipation. In all simulations, the wave height is set to $H_w = 0.075m$

The numerical setup, domain dimensions, and grid resolution are the same as in the validation case.

Fig. 4 and Fig. 5 present 3D views of the wave collapsing as well as the run-up process for the waves with $T = 0.8s$. The water surface is shown in blue, and isosurfaces of the Q criterion are added to visualize turbulence structures. In $case1_{08}$ the edge of the structure used in $case2_{08}$ is drawn as reference. In Fig. 4 the collapsing stage of the wave is observed; it can be seen that in $case1_{08}$ a more predominant water tongue is formed, in comparison to $case2_{08}$, where a more compact breaking is generated. The turbulence in $case1_{08}$ have more significant structures. However, a greater number of vortices are observed in $case2_{08}$. Fig 5 presents the first instances of the run-up process. A more turbulent flow is observed in $case1_{08}$, where long vortices are observed, whereas, in $case2_{08}$, most of the vortices are too weak to be captured with the chosen isosurface value. A slower run-up flow is also observed in $case1_{08}$; at $t = 10.58s$, the water tongue in $case2_{08}$ reaches the crest of the structure, but at the same time interval in $case1_{08}$ is still below that level. These different behaviours give indications that a more significant run-down flow affects the energy dissipation.

Fig. 6 and Fig. 7 show the collapsing and run-up process for the wave with $T = 1.0s$. In these simulations, the differences between the cases are not as

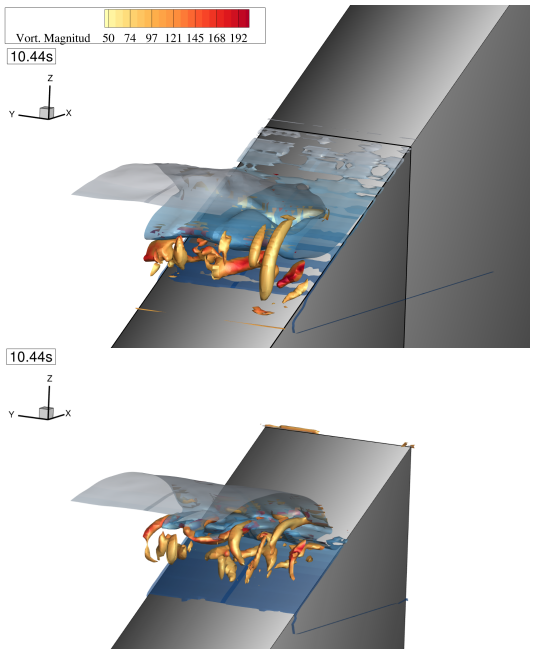

Fig. 4. 3D views wave collapsing $t = 10.44s$. Top figure case1_{08}, and bottom figure case2_{08}. Water surface in blue and iso-surface of Q criterion=1,500 coloured by vortex magnitude.

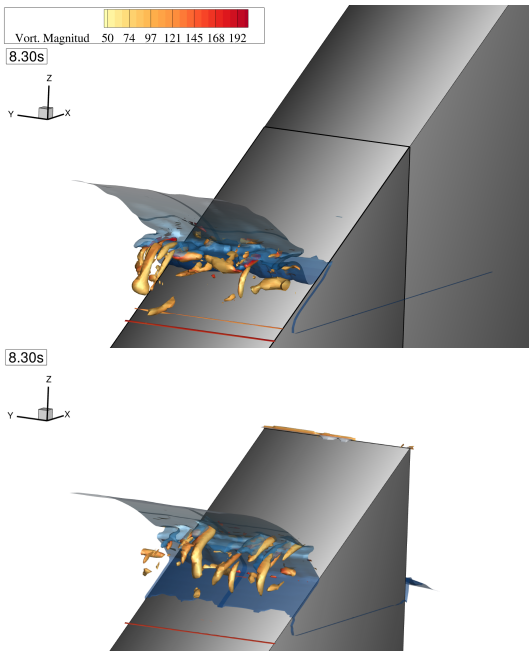

Fig. 6. 3D views wave collapsing $t = 8.30s$. Top figure case1_{10}, and bottom figure case2_{10}. Water surface in blue and iso-surface of Q criterion=1,500 coloured by vortex magnitude.

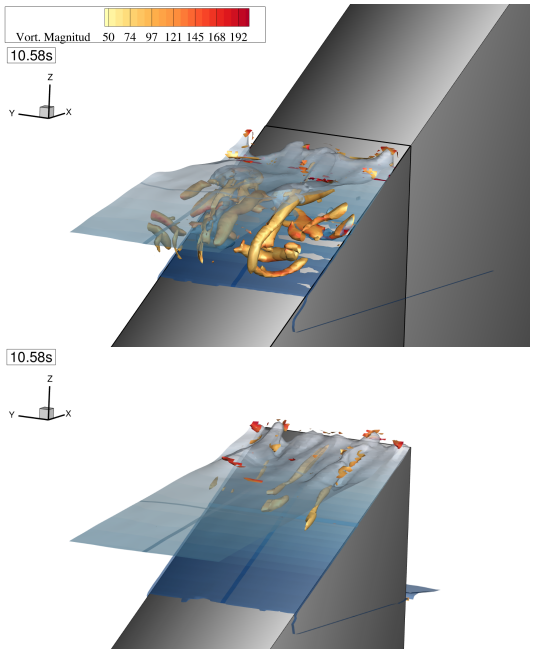

Fig. 5. 3D views run-up $t = 10.58s$. Top figure case1_{08}, and bottom figure case2_{08}. Water surface in blue and iso-surface of Q criterion=1,500 coloured by vortex magnitude.

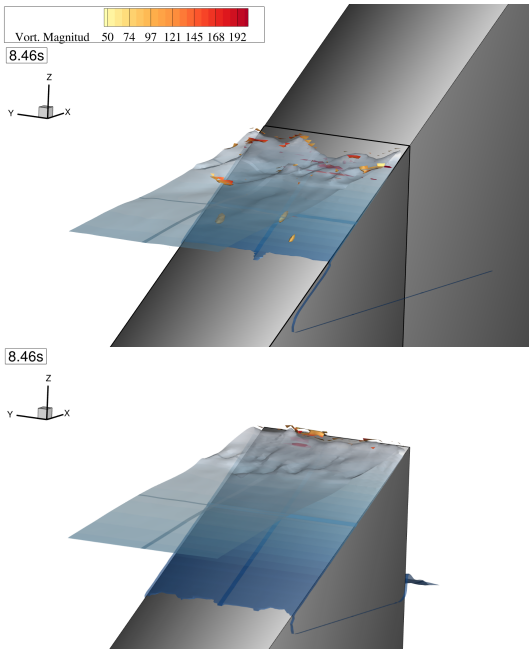

Fig. 7. 3D views of the wave run-up $t = 8.46s$. Top figure case1_{10}, and bottom figure case2_{10}. Water surface in blue and iso-surface of Q criterion=1,5 coloured by vorticity magnitude.

significant as in the shorter waves. Fig. 6 shows slightly bigger vortices than in case1_{10}. Both cases show a small water tongue at the front of the wave and an almost vertical shape near the structure's surface. In Fig. 7, it can be observed that the vortices are dissipated almost completely and only a few are observed in case1_{10}. A slower run-up flow is also detected in case1_{10} similar to the shorter wave.

The flow's energies are evaluated in two control cross sections which are, $S1$ at $x = 0.10m$, and $S2$ at $x = 5.93m$ and $z = 0.317m$, Fig. 8. The former is used to calculate the incoming wave energy (E_w), and the latter, located after the breaking zone, which allows to evaluate the energy during the run-up and backwash flows. The flow's kinetic (KE), dynamic potential (DPE) and total energy (TE) are calculated according to (14), (15) and (16). DPE represents the potential energy generated only due to the action of the waves and is calculated as the total potential energy of the flow minus the potential energy in still water level (SWL) condition.

$$KE = \int_0^T \int_0^{L_y} \int_0^{\eta(t)} 0.5\rho(u^2 + v^2 + w^2)\, dz\, dy\, dt \quad (14)$$

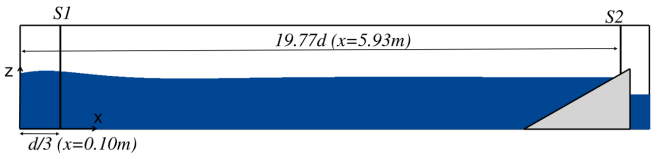

Fig. 8. Longitudinal view of the domain and sections S1, and S2 where energy is calculated.

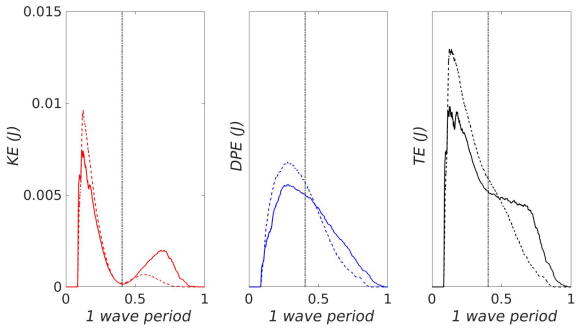

Fig. 9. Energy over one wave period at section S2. Left: Kinetic energy, centre: Dynamic potential energy, right: Total energy. Solid lines Case1$_{08}$, dashed line Case2$_{08}$.

$$DPE = \int_0^T \int_0^{L_y} \int_0^{\eta(t)} \rho g z \, dz \, dy \, dt - \left[\int_0^T \int_0^{L_y} \int_0^{\eta(t)} \rho g z \, dz \, dy \, dt \right]^{\text{at SWL}} \quad (15)$$

$$TE = KE + DPE \quad (16)$$

Where u, v and w are the velocity components, $\eta(t)$ is the variable water surface measure from the bottom and L_y is the width of the domain. The incoming total wave energy (E_w) is calculated in section $S1$ for one period.

Fig. 9 shows profiles of KE, DPE, and TE over one wave period at S2, for Case1$_{08}$ and Case2$_{08}$. The variation of the Kinetic energy allows to identify two distinct events (the run-upo and the backwash), separated by the vertical line at 0.4. This line represents the time when the run-up finishes (left side of the plots) and the backwash starts (right side of the plots). It can be seen that in all plots Case2$_{08}$ higher peaks of energy during the run-up stage is achieved. On the other hand, Case1 presents a larger level of energy during the run-down phase. These differences are due to a decrease in the run-down flow because of the occurrence of overtopping in Case2.

Fig. 10 shows the energy variation, normalized by the wave energy (E_w), for 8 waves during the run-up stage in $S2$ for the $T = 0.8$ waves. Case1 is presented in solid lines and Case2 with dashed lines. It can be seen that in all waves, the total energy, and dynamic potential energy, black and blue lines, respectively, are greater for Case2. A smaller increment is appreciated in the Kinetic energy of the run-up flow, especially in the 7^{th} and 8^{th}, where both cases have similar values. The variation between Case1 and Case2 is also shown in Fig. 11, where the energies are average for the eight

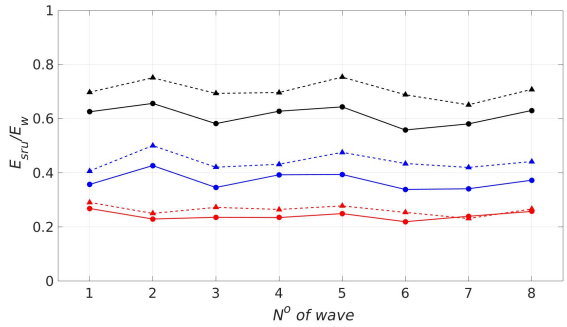

Fig. 10. Kinetic energy, red, dynamic potential energy, blue, and total energy, black, in section S2 for waves $T = 0.8s$ during run-up stage averaged over eight waves and normalized by the wave energy Ew. Case 1 solid line, case 2 dashed line.

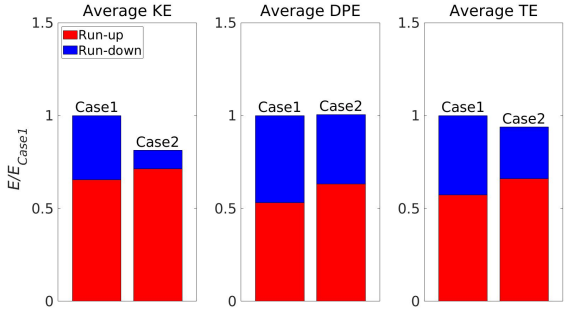

Fig. 11. Average energy in section S2, separated by run-up, red bars, and run-down, blue bars, for waves $T = 0.8s$, and normalized by energy measured in case 1.

waves shown in 10 and normalized by Case1. It can be seen that the energy in the run-down process, blue bar, decreases due to the occurrence of overtopping in Case2, which reduces the run-down. Focusing on the run-up process, red bars, the kinetic energy present an average increment of 5.94%, the dynamic potential grows by 10.13%, and the total energy by 8.67%. These changes are directly related to the differences in the turbulence structures detected in Fig. 4 and Fig. 5. The generation of overtopping decreases the backwash reducing energy losses during the collapsing of the waves.

Fig. 12 shows the same analysis as in Fig. 10 but for the longer waves, $T = 1.0s$. It can be seen that the energy variation between Case1 and Case2 are not as significant as for the shorter waves, especially in the kinetic energy where no significant variation is detected. Fig. 13 shows the energy average variation normalized by Case1. In the run-up process, the kinetic energy in Case2 experiences a reduction of 2.32%, the dynamic potential increases a 6.13%, and the total energy grows by 3.34%. These minor variations are aligned with the smaller differences in the turbulence levels observed in Fig. 6 and Fig. 7.

V. Conclusions and Further Work

The present work has studied the effect of backwash flow on energy dissipation during the wave collapse and run-up processes over an impermeable sloped structure, representing the run-up ramp of an OWEC.

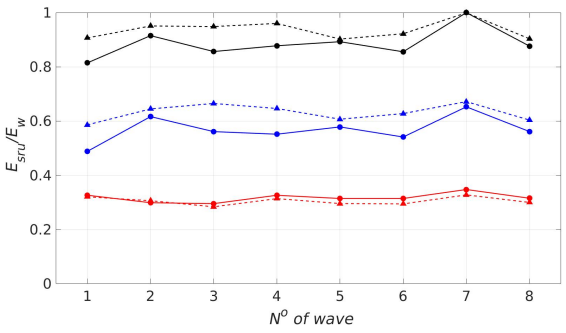

Fig. 12. Variation of kinetic energy, red, dynamic potential energy, blue, and total energy, black, in section S2 for waves $T = 1.0s$ during run-up stage for eight waves and normalized by the wave energy Ew. Case 1 solid line, case 2 dashed line.

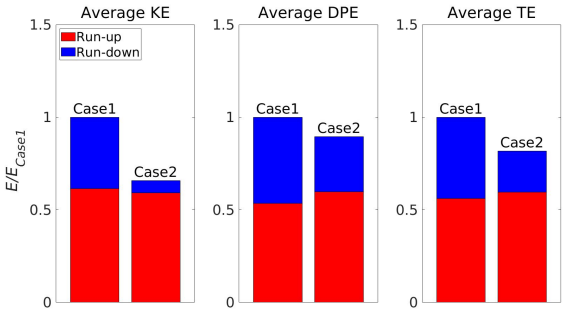

Fig. 13. Average energy in section S2, separated by run-up, red bars, and run-down, blue bars, for waves $T = 1.0s$, and normalized by energy measured in case 1.

Two cases have been considered, one where only run-up has occurred (case 1), and a second where overtopping has taken place by reducing the freeboard crest of the structure (case 2). The overtopping in the second case generates a reduction in the backwash flow, permitting to study of its effect on energy dissipation. The energy has been quantified in a section downstream of wave breaking.

Two wave conditions with the best agreement with the laboratory data have been used to validate Hydro3D's performance to reproduce overtopping discharges. In total 4 simulations were generated, two cases for each wave condition.

Differences in the turbulence structures between cases 1 and 2 have been observed. The shorter wave shows a significant reduction in the flow turbulence when overtopping is allowed, especially at the beginning of the run-up event when a more turbulent flow is appreciated in case 1. For the longer wave, the differences between both cases are not as significant as for the shorter wave; only a slight reduction of the turbulence level is found with a reduced backwash.

The differences in the flow turbulence also shows in the energy during the run-up events. Both wave conditions exhibit an increment in the energy when a reduced backwash occurs by allowing overtopping. The energy growth is more significant in the shorter wave, as expected, due to more significant turbulence variation found between case 1 and 2.

These findings show that a reduction of the backwash flow helps to decrease the energy dissipation during the breaking of the approaching wave. This leads to a reduction of the amount of water running down the slope, which acts in the opposite direction to the incoming wave contributing to increased turbulence. These results give indications that a reduction in the backwash flow could improve the efficiency of an OWEC.

Further work will focus on expanding the wave conditions studied to verify if longer waves are less affected by changes in the backwash flow. In addition, more cases will be conducted for each wave condition to identify the function that relates the energy increment with the variation of the backwash flows.

VI. Nomenclature

Acronyms

- CDS: Central differences scheme.
- CFL: Courant-Friedrichs-Lewy condition.
- DPE: Dynamic potential energy.
- IB: Immersed boundary method.
- KE: Kinetic energy.
- LES: Large Eddy Simulation.
- LSM: Level-set method.
- OWEC: Overtopping wave energy converter.
- OWC: Oscillating water columns.
- RK: Runge-Kutta scheme.
- RM: Relaxation method.
- SGS: Sub-grid scale model.
- SWL: Still water level.
- TE: Total energy.
- WALE: Wall-Adapting Local Eddy-viscosity.
- WENO: 5^{th} order Weighted essentially non-oscillatory scheme.

Symbols

- C_w: WALE empirical constant.
- d: Water depth in still water condition (m).
- dx, dy, dz: Grid size in x, y and z direction respectively (m).
- $\delta(\phi)$: Transition function used to calculate F_i^{sf}.
- 2ε: Thickness transition zone used in LSM.
- H_w: Wave height (m) in inlet boundary.
- $H(\phi)$: Heaviside function used in LSM.
- L_w: Wave length (m) in inlet boundary.
- $\eta(t)$: Variable water depth (m).
- κ: Interface curvature used to calculate F_i^{sf}.
- f_i: Forcing calculated by IB.
- F_i^{sf}: Surface tension.
- g_i: Gravitational acceleration.
- $\bar{p}$: Pressure field.
- u: Velocity in x direction.
- $\bar{u}_i$: Instantaneous filter velocity.
- ν: Fluid kinematic viscosity.
- ν_t: Fluid viscosity calculated by SGS.
- ρ: Fluid density.
- q: Overtopping mean discharge.
- Q: Dimensionless overtopping mean discharge.
- σ: Surface tension coefficient.
- R: Relaxation method coefficient.
- T: Wave period (s).

- τ_{ij}^{SGS}: Sub-grid scale stress tensor.
- ϕ: Distance function used in LSM to capture water surface.
- v: Velocity in y direction.
- w: Velocity in z direction.
- $\Gamma(x_r)$: Relaxation function used in RM.
- Δ: Filtered size used in WALE, defined as $(dx \cdot dy \cdot dz)$.

REFERENCES

[1] A. F. O. Falcão, "Wave energy utilization: A review of the technologies," pp. 899–918, 4 2010.

[2] Y. Zhang, Y. Zhao, W. Sun, and J. Li, "Ocean wave energy converters: Technical principle, device realization, and performance evaluation," 5 2021.

[3] K. Gunn and C. Stock-Williams, "Quantifying the global wave power resource," *Renewable Energy*, vol. 44, pp. 296–304, 8 2012.

[4] C. Iuppa, P. Contestabile, L. Cavallaro, E. Foti, and D. Vicinanza, "Hydraulic performance of an innovative breakwater for overtopping wave energy conversion," *Sustainability (Switzerland)*, vol. 8, 2016.

[5] Z. Liu, Z. Han, H. Shi, and W. Yang, "Experimental study on multi-level overtopping wave energy convertor under regular wave conditions," *International Journal of Naval Architecture and Ocean Engineering*, vol. 10, pp. 651–659, 9 2018.

[6] P. Oliveira, F. Taveira-Pinto, T. Morais, and P. Rosa-Santos, "Experimental evaluation of the effect of wave focusing walls on the performance of the sea-wave slot-cone generator," *Energy Conversion and Management*, vol. 110, pp. 165–175, 2 2016.

[7] M. A. Musa, M. F. Roslan, M. F. Ahmad, A. M. Muzathik, M. A. Mustapa, A. Fitriadhy, M. H. Mohd, and M. A. Rahman, "The influence of ramp shape parameters on performance of overtopping breakwater for energy conversion," *Journal of Marine Science and Engineering*, vol. 8, pp. 1–18, 11 2020.

[8] T. W. Hsu, S. J. Liang, B. D. Young, and S. H. Ou, "Nonlinear run-ups of regular waves on sloping structures," *Natural Hazards and Earth System Science*, vol. 12, pp. 3811–3820, 2012.

[9] A. Christou, T. Stoesser, and Z. Xie, "A large-eddy-simulation-based numerical wave tank for three-dimensional wave-structure interaction," *Computers and Fluids*, vol. 231, 12 2021.

[10] A. Christou, Z. Xie, T. Stoesser, and P. Ouro, "Propagation of a solitary wave over a finite submerged thin plate," *Applied Ocean Research*, vol. 106, 1 2021.

[11] C.-W. Shu, "High order weighted essentially nonoscillatory schemes for convection dominated problems," *SIAM Review*, vol. 51, no. 1, pp. 82–126, 2009. [Online]. Available: https://doi.org/10.1137/070679065

[12] A. J. Chorin, "Numerical solution of the Navier-Stokes equations," *Mathematics of Computation*, vol. 22, no. 104, pp. 745–745, 1968.

[13] F. Nicoud and F. Ducros, "Subgrid-scale stress modelling based on the square of the velocity gradient tensor," *Flow, Turbulence and Combustion*, vol. 62, pp. 183–200, 1999.

[14] S. Osher and J. A. Sethian, "Fronts propagating with curvature-dependent speed: Algorithms based on Hamilton-Jacobi formulations," *Journal of Computational Physics*, vol. 79, no. 1, pp. 12–49, 1988.

[15] M. Uhlmann, "An immersed boundary method with direct forcing for the simulation of particulate flows," *Journal of Computational Physics*, vol. 209, pp. 448–476, 11 2005.

[16] K. Yokoi, R. Onishi, X. L. Deng, and M. Sussman, "Density-scaled balanced continuum surface force model with a level set based curvature interpolation technique," *International Journal of Computational Methods*, vol. 13, 8 2016.

[17] Z. Han, Z. Liu, and H. Shi, "Numerical study on overtopping performance of a multi-level breakwater for wave energy conversion," *Ocean Engineering*, vol. 150, pp. 94–101, 2 2018.